

Synthesis, Structure, Spectroscopic Properties, and Antiproliferative Activity In Vitro of Novel Osmium(III) Complexes with Azole Heterocycles[§]

Iryna N. Stepanenko, Artem A. Krokhin, Roland O. John, Alexander Roller, Vladimir B. Arion,*
Michael A. Jakupec, and Bernhard K. Keppler*

University of Vienna, Institute of Inorganic Chemistry, Währingerstr. 42, A-1090 Vienna, Austria

Received April 18, 2008

Reactions of $(\text{H}_2\text{azole})_2[\text{OsCl}_6]$, where Hazole = pyrazole, Hpz, (**1**), indazole, Hind, (**2**), imidazole, Him, (**3**) and benzimidazole, Hbzim, (**4**) with the corresponding azole heterocycle in 1:4 molar ratio in boiling isoamyl alcohol or hexanol-1 afforded novel water-soluble osmium(III) complexes of the type *trans*- $[\text{OsCl}_2(\text{Hazole})_4]\text{Cl}$, where Hazole = Hpz (**5a**), Hind (**6a**), Him (**7a**), and Hbzim (**9a**) in 50–70% (**5a**, **7a**, **9a**) and 5% (**6a**) yields. The synthesis of **7a** was accompanied by a concurrent reaction which led to minor formation (<4%) of *cis*- $[\text{OsCl}_2(\text{Him})_4]\text{Cl}$ (**8**). The complexes were characterized by elemental analysis, IR spectroscopy, UV–vis spectroscopy, ESI mass spectrometry, cyclic voltammetry, and X-ray crystallography. **5a**, **7a**, and **9a** were found to possess remarkable antiproliferative activity in vitro against A549 (non-small cell lung carcinoma), CH1 (ovarian carcinoma), and SW480 (colon carcinoma) cells, which was compared with that of related ruthenium compounds *trans*- $[\text{RuCl}_2(\text{Hazole})_4]\text{Cl}$, where Hazole = Hpz (**5b**), Hind (**6b**), Him (**7b**), and Hbzim (**9b**).

Introduction

The compounds $(\text{H}_2\text{im})[\text{trans-Ru}^{\text{III}}\text{Cl}_4(\text{Him})(\text{DMSO})]$ (NAMI-A, Him = imidazole) and $(\text{H}_2\text{ind})[\text{trans-Ru}^{\text{III}}\text{Cl}_4(\text{Hind})_2]$ (KP1019, Hind = indazole) were selected for clinical development as anticancer agents from a large number of ruthenium complexes.^{1–10} Whereas KP1019 is active against malignant tumors (in particular, colon carcinoma) and their metastases, NAMI-A was shown to be less cytotoxic in cell cultures but able to inhibit the formation of metastases.

It is generally believed that the activity of ruthenium(III) complexes depends on their reduction in vivo to more labile ruthenium(II) complexes. Such a reduction has been reported to occur under the hypoxic conditions in solid tumors.^{11–14} The resulting ruthenium(II) species show a higher propensity for ligand exchange reactions and might therefore interact with target molecules more rapidly. Their cytotoxicity often correlates with the DNA binding ability.^{5,11,15,16}

The correlation between cytotoxicity and electrochemical properties for $[\text{Ru}^{\text{III}}\text{Cl}_{(6-n)}(\text{Hind})_n]^{(3-n)-}$ ($n = 0–4$) compounds was reported previously.¹⁷ Reduction potentials, both

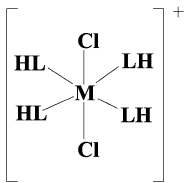
calculated according to Lever's parametrization method and measured by cyclic voltammetry, showed that a higher indazole-to-chloride ratio results in a higher reduction potential. The antiproliferative activity of these compounds in colon cancer cells (SW480) and ovarian cancer cells (CH1) varied broadly, but largely correlated with their $\text{Ru}^{\text{III}}/\text{Ru}^{\text{II}}$ redox potentials in the following order: $[\text{Ru}^{\text{III}}\text{Cl}_6]^{3-} < [\text{Ru}^{\text{III}}\text{Cl}_4(\text{Hind})_2]^- < [\text{Ru}^{\text{III}}\text{Cl}_5(\text{Hind})]^{2-} < [\text{Ru}^{\text{III}}\text{Cl}_3(\text{Hind})_3]^- < [\text{Ru}^{\text{III}}\text{Cl}_2(\text{Hind})_4]^+ \approx [\text{Ru}^{\text{II}}\text{Cl}_2(\text{Hind})_4]$.¹⁷ A similar relationship between $\text{Ru}^{\text{III}}/\text{Ru}^{\text{II}}$ redox potentials and cytotoxic potency in the SW480 cell line was observed for (H_2azole) - $[\text{trans-Ru}^{\text{III}}\text{Cl}_4(\text{Hazole})_2]$ complexes, where Hazole = imidazole, 1,2,4-triazole and indazole.^{18,19}

In addition, the interest in osmium complexes as potential antitumor agents is growing,^{16,20–25} and a recent comparative study on ruthenium(III) NAMI-A-type complexes and their osmium(III) analogues revealed that the latter have reasonable antiproliferative activity in vitro in two human cancer cell lines, HT-29 (colon carcinoma) and SK-BR-3 (mammary carcinoma), with IC_{50} values mostly in the 10^{-5} M range.²⁶ It is therefore worthwhile (i) to develop synthetic routes to osmium congeners of the complexes $[\text{Ru}^{\text{III}}\text{Cl}_2(\text{Hazole})_4]\text{Cl}$ ¹⁷ (Hazole = azole heterocycle) with 2:1 Hazole-to-chloride stoichiometry at the metal center, which were found to

* To whom correspondence should be addressed. E-mail: vladimir.arion@univie.ac.at (V.B.A.), bernhard.keppler@univie.ac.at (B.K.K.). Fax: +43 1 427752680.

[§] Dedicated to Prof. Jan Reedijk on the occasion of his 65th birthday.

Chart 1. Anticancer $[M^{III}Cl_2(Hazole)_4]Cl$ complexes; underlined complexes have been characterized in this work by X-ray crystallography

	Complex	M	HL
$(H_2L)_2[MCl_6]$	1	Os	Hpz
	2	Os	Hind
	3	Os	Him
	4	Os	Hbzim
	<u>5a</u>	Os	Hpz
	<u>5b</u>	Ru	Hpz
	<u>6a</u>	Os	Hind
	<u>6b</u>	Ru	Hind
	<u>7a</u>	Os	Him
	<u>7b</u>	Ru	Him
	<u>9a</u>	Os	Hbzim
	<u>9b</u>	Ru	Hbzim

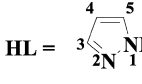
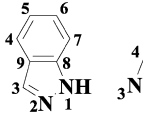
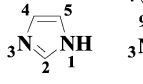
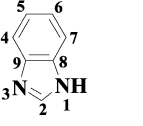
			
pyrazole (Hpz)	indazole (Hind)	imidazole (Him)	benzimidazole (Hbzim)

exhibit the highest cytotoxicity within a series of indazole complexes (vide supra); (ii) to study their structure, spectroscopic properties, electrochemical behavior, aqueous stability, and DNA base binding ability; (iii) to evaluate their antiproliferative activity in vitro in human cancer cell lines in comparison to relevant *trans*- $[Ru^{III}Cl_2(Hazole)_4]Cl$ complexes; and (iv) to elucidate relationships between Os^{III}/Os^{II} redox potentials and cytotoxicity of the prepared complexes.

In this article, we show that a number of *trans*- $[Os^{III}Cl_2(Hazole)_4]Cl$ complexes, where Hazole = pyrazole, Hpz, (**5a**), indazole, Hind, (**6a**), imidazole, Him, (**7a**), and benzimidazole, Hbzim, (**9a**), can be prepared as major isomers (Chart 1) when starting from $(H_2azole)_2[Os^{IV}Cl_6]$ (**1–4**) and an excess of azole heterocycle. However, formation of cis isomers as minor products is also possible, as found by the isolation and characterization of **8**. Comprehensive characterization of the prepared complexes and their biological evaluation as potential anticancer agents provides the basis for a comparison with the previously reported ruthenium(III) complexes *trans*- $[Ru^{III}Cl_2(Hazole)_4]Cl$ (**5b**, **6b**, **7b**, and **9b**).^{17,19}

Experimental Section

Materials. The starting compound $[(DMSO)_2H]_2[OsCl_6]$ was synthesized as previously reported in the literature.^{27,28} OsO_4 (99.8%) and $N_2H_4 \cdot 2HCl$ were purchased from Johnson Matthey and Fluka, correspondingly. Pyrazole, indazole, imidazole, and benzimidazole were from Aldrich and Fluka. The synthesis of $[OsCl_2(Hazole)_4]Cl$ was performed under an argon atmosphere by using standard Schlenk techniques. *trans*- $[Ru^{III}Cl_2(Hazole)_4]Cl$ (Hazole = Hpz (**5b**), Him (**7b**), Hbzim (**9b**)) were synthesized according to the literature protocols.¹⁹

- Galanski, M.; Arion, V. B.; Jakupec, M. A.; Keppler, B. K. *Curr. Pharm. Des.* **2003**, *9*, 2078–2089.
- Alessio, E.; Mestroni, G.; Bergamo, B.; Sava, G. *Curr. Top. Med. Chem.* **2004**, *4*, 1525–1535.
- Hartinger, Ch. G.; Zorbas-Seifried, S.; Jakupec, M. A.; Kynast, B.; Zorbas, H.; Keppler, B. K. *J. Inorg. Biochem.* **2006**, *100*, 891–904.
- Rademaker-Lakhai, J. M.; Van Den Bongard, D.; Pluim, D.; Beijnen, J. H.; Schellens, J. H. M. *Clin. Cancer Res.* **2004**, *10*, 3717–3727.
- Jakupec, M. A.; Galanski, M.; Arion, V. B.; Hartinger, C. G.; Keppler, B. K. *Dalton Trans.* **2008**, *2*, 183–194.
- Groessler, M.; Reisner, E.; Hartinger, C. G.; Eichinger, R.; Semenova, O.; Timerbaev, A. R.; Jakupec, M. A.; Arion, V. B.; Keppler, B. K. *J. Med. Chem.* **2007**, *50*, 2185–2193.
- Bratsos, I.; Jedner, S.; Gianferrara, T.; Alessio, E. *Chimia* **2007**, *61*, 692–697.
- Cini, R.; Tamasi, G.; Defazio, S.; Corsini, M.; Zanello, P.; Messori, L.; Marcon, G.; Piccioli, F.; Orioli, P. *Inorg. Chem.* **2003**, *42*, 8038–8052.
- Kennedy, D. C.; Wu, A.; Patrick, B. O.; James, B. R. *J. Inorg. Biochem.* **2006**, *100*, 1974–1982.
- Huxham, L. A.; Cheu, E. L. S.; Patrick, B. O.; James, B. R. *Inorg. Chim. Acta* **2003**, *352*, 238–246.
- Clarke, M. J. *Coord. Chem. Rev.* **2003**, *236*, 209–233.
- Clarke, M. J.; Zhu, F.; Frasca, D. R. *Chem. Rev.* **1999**, *99*, 2511–2533.

- Clarke M. J. In *Metal Complexes in Cancer Chemotherapy*; Keppler B. K., Ed.; VCH: Weinheim, 1993; 129–157.
- Mestroni, G.; Alessio, E.; Sava, G.; Pacor, S.; Coluccia, M. In *Metal Complexes in Cancer Chemotherapy*; Keppler B. K., Ed.; VCH: Weinheim, 1993; 157–185.
- Romerosa, A.; Saoud, M.; Campos-Malpartida, T.; Lidrissi, C.; Serrano-Ruiz, M.; Peruzzini, M.; Garrido, J. A.; Garcia-Maroto, F. *Eur. J. Inorg. Chem.* **2007**, *18*, 2803–2812.
- (a) Ronconi, L.; Sadler, P. J. *Coord. Chem. Rev.* **2007**, *251*, 1633–1648. (b) Kostrhunova, H.; Florian, J.; Novakova, O.; Peacock, A. F. A.; Sadler, P. J.; Brabec, V. *J. Med. Chem.* **2008**, *51*, 3635–3643.
- Jakupec, M. A.; Reisner, E.; Eichinger, A.; Pongratz, M.; Arion, V. B.; Galanski, M.; Hartinger, Ch. G.; Keppler, B. K. *J. Med. Chem.* **2005**, *48*, 2831–2837.
- Reisner, E.; Arion, V. B.; Guedes da Silva, M. F. C.; Lichtenecker, R.; Eichinger, A.; Keppler, B. K.; Kukushkin, V. Yu.; Pombeiro, A. J. L. *Inorg. Chem.* **2004**, *43*, 7083–7093.
- Reisner, E.; Arion, V. B.; Eichinger, A.; Kandler, N.; Giester, G.; Pombeiro, A. J. L.; Keppler, B. K. *Inorg. Chem.* **2005**, *44*, 6704–6716.
- Peacock, A. F. A.; Habtemariam, A.; Moggach, S. A.; Prescimone, A.; Parsons, S.; Sadler, P. J. *Inorg. Chem.* **2007**, *46*, 4049–4059.
- Dorcier, A.; Ang, W. H.; Bolano, S.; Gonsalvi, L.; Juillerat-Jeannerat, L.; Laurenczy, G.; Peruzzini, M.; Phillips, A. D.; Zanobini, F.; Dyson, P. J. *Organometallics* **2006**, *25*, 4090–4096.
- Dorcier, A.; Dyson, P. J.; Gossens, C.; Rothlisberger, U.; Scopelliti, R.; Tavernelli, I. *Organometallics* **2005**, *24*, 2114–2123.
- Dougan, S. J.; Sadler, P. J. *Chimia* **2007**, *61*, 704–715.
- Peacock, A. F. A.; Habtemariam, A.; Fernández, R.; Walland, V.; Fabbiani, F. P. A.; Parsons, S.; Aird, R. E.; Jodrell, D. I.; Sadler, P. J. *J. Am. Chem. Soc.* **2006**, *128*, 1739–1748.
- Dyson, P. J. *Chimia* **2007**, *61*, 698–703.
- Cebrian-Losantos, B.; Krokhin, A. A.; Stepanenko, I. N.; Eichinger, R.; Jakupec, M. A.; Arion, V. B.; Keppler, B. K. *Inorg. Chem.* **2007**, *46*, 5023–5033.
- Brauer, G. *Handbuch der Präparativen Anorganischen Chemie*, III **1981**, 1742–1744.
- Rudnitskaya, O. V.; Buslaeva, T. M.; Lyalina, N. N. *Zh. Neorg. Khim.* **1994**, *39*, 922–924.

(H₂pz)₂[OsCl₆] (1). To a solution of [(DMSO)₂H]₂[OsCl₆] (997.6 mg, 1.4 mmol) in dry ethanol (20 mL) an excess of pyrazole (267.9 mg, 3.9 mmol) was added. This suspension was stirred at room temperature for 2 h and then concentrated under reduced pressure to a minimal volume. The solution above the precipitate was decanted, and the product was washed with diethyl ether (2 × 5 mL) and dried in vacuo at 60–70 °C for 24 h. Yield: 693 mg, 92%. Anal. Calcd for C₆H₁₀Cl₆N₄Os (*M_r* = 541.09 g/mol): C, 13.32; H, 1.86; N, 10.35. Found: C, 13.17; H, 2.05; N, 10.12. IR spectrum in KBr, cm⁻¹: 517, 608, 637, 795, 872, 919, 1052, 1102, 1165, 1233, 1318, 1404, 1461, 1519, 1546, 1596, and 1716 ν(C–C), ν(C–N) and σ(C–H); 2746, 2851, 2926, 3136, 3249, 3499, and 3562 ν(C–H) and ν(N–H). UV–vis (CH₃OH), λ_{max}, nm (ε, M⁻¹ cm⁻¹): 215 (22 374), 253 sh (2233), 276 sh (1161), 302 sh (1219), 336 (7614), 347 (7495), 371 (7060), 422 (869). ¹H NMR (400 MHz, *d*₆-DMSO): δ 7.68 (s, 2H, H₃ and H₅), 6.31 (s, 1H₄) ppm.

(H₂ind)₂[OsCl₆] (2). The complex was prepared as an orange powder by following a procedure analogous to that reported above for **1**, starting from [(DMSO)₂H]₂[OsCl₆] (1005.7 mg, 1.4 mmol) and indazole (484.7 mg, 4.1 mmol) in dry ethanol (20 mL). Yield: 709.2 mg, 79%. Anal. Calcd for C₁₄H₁₄Cl₆N₄Os (*M_r* = 641.21 g/mol): C, 26.22; H, 2.20; N, 8.74. Found: C, 26.11; H, 2.50; N, 8.69. IR spectrum in KBr, cm⁻¹: 429, 538, 611, 643, 756, 831, 893, 928, 962, 997, 1093, 1239, 1263, 1312, 1369, 1385, 1451, 1526, 1549, 1605, 1638, 1722, 1818, 1955, and 1991 ν(C–C), ν(C–N) and σ(C–H); 2676, 2735, 2842, 2880, 2953, 3014, 3142, and 3472 ν(C–H) and ν(N–H). UV–vis (CH₃OH), λ_{max}, nm (ε, M⁻¹ cm⁻¹): 211 (52 780), 251 (10 611), 258 sh (9610), 285 (9132), 337 (8551), 349 (8356), 371 (7909), 421 (994). ¹H NMR (400 MHz, *d*₆-DMSO): 8.06 (s, 1H₃), 7.76 (d, *J* = 8.36 Hz, 1H₄ or 1H₇), 7.53 (d, *J* = 8.6 Hz, 1H₄ or 1H₇), 7.34 (t, *J* = 7.7 Hz, 1H₅ or 1H₆), 7.10 (t, *J* = 7.58 Hz, 1H₅ or 1H₆) ppm.

(H₂im)₂[OsCl₆] (3). The complex was prepared as an orange powder by following a procedure analogous to that reported above for **1**, starting from [(DMSO)₂H]₂[OsCl₆] (225.7 mg, 0.32 mmol) and imidazole (64.6 mg, 0.95 mmol) in dry ethanol (10 mL). Yield: 153.4 mg, 90%. Anal. Calcd for C₆H₁₀Cl₆N₄Os (*M_r* = 541.09 g/mol): C, 13.32; H, 1.86; N, 10.35. Found: C, 13.49; H, 1.69; N, 10.12. IR spectrum in KBr, cm⁻¹: 620, 690, 773, 884, 922, 1046, 1085, 1107, 1162, 1189, 1304, 1421, 1438, 1529, 1578, 1636, and 1757 ν(C–C), ν(C–N), and σ(C–H); 3035, 3129, 3163, 3249, and 3316 ν(C–H) and ν(N–H). UV–vis (CH₃OH), λ_{max}, nm (ε, M⁻¹ cm⁻¹): 216 (19 809), 256 sh (1621), 279 sh (662), 303 sh (838), 336 (8277), 346 (8194), 371 (7668), 423 (879). ¹H NMR (400 MHz, *d*₆-DMSO): δ 14.22 (s, H_{NH}), 9.07 (s, 1H₂), 7.69 (s, 2H, H₄ and H₅) ppm.

(H₂bzim)₂[OsCl₆] (4). The preparation of **4** as an orange powder was carried out following the procedure used for the synthesis of **1**, starting from [(DMSO)₂H]₂[OsCl₆] (711.5 mg, 0.99 mmol) and benzimidazole (328.9 mg, 2.8 mmol) in dry ethanol (25 mL). Yield: 618.4 mg, 97%. Anal. Calcd for C₁₄H₁₄Cl₆N₄Os (*M_r* = 641.21 g/mol): C, 26.22; H, 2.20; N, 8.74. Found: C, 25.96; H, 2.48; N, 8.49. IR spectrum in KBr, cm⁻¹: 418, 507, 542, 598, 622, 702, 757, 861, 866, 939, 966, 1005, 1110, 1137, 1238, 1266, 1384, 1447, 1498, 1507, 1596, 1621, 1734, 1845, 1931, and 1968 ν(C–C), ν(C–N) and σ(C–H); 2752, 2811, 2958, 3041, 3157, 3260, 3516, and 3581 ν(C–H) and ν(N–H). UV–vis (CH₃OH), λ_{max}, nm (ε, M⁻¹ cm⁻¹): 211 (22 098), 222 sh (13 896), 267 (8796), 274 (8830), 336 (5786), 346 (5691), 372 (5326), 423 (655). ¹H NMR (400 MHz, *d*₆-DMSO): δ 9.43 (s, 1H₂), 7.84 (d, *J* = 6.08 Hz, 1H₄ or 1H₇), 7.83 (d, *J* = 6.32 Hz, 1H₄ or 1H₇), 7.57 (d, *J* = 6.28 Hz, 1H₅, or 1H₆), 7.56 (d, *J* = 6.32 Hz, 1H₅ or 1H₆) ppm.

trans-[OsCl₂(Hpz)₄]Cl (5a). Pyrazole (100 mg, 1.47 mmol) was added to a suspension of **1** (195 mg, 0.36 mmol) in hexanol-1 (10 mL), and the mixture was heated at 170 °C for 24 h. After the reaction mixture was allowed to cool to room temperature, the alcohol was evaporated under reduced pressure at 60 °C. Addition of diethyl ether (15–20 mL) to the oily residue and treatment of the mixture in an ultrasound bath for 1.5 h afforded a brown precipitate. This was filtered off, dried in vacuo, and purified by column chromatography on silica, using as eluent a mixture of CHCl₃/CH₃OH (5:1) and collecting the second fraction (*R_f* = 0.68). The complex crystallized as dark-red crystals by diffusion of diethyl ether into a methanol solution of **5a** and dried under nitrogen at 140 °C for 1 h. Yield: 105 mg, 50%. Anal. Calcd for C₁₂H₁₆Cl₃N₈Os (*M_r* = 568.90 g/mol): C, 25.33; H, 2.83; N, 19.70. Found: C, 25.05; H, 2.80; N, 19.45. ESI-MS in MeOH (positive), *m/z*: 534.2 [OsCl₂(Hpz)₄]⁺, ESI-MS in MeOH (negative), *m/z*: 392.7 [OsCl₂(Hpz)₂–2H]⁻. IR spectrum in KBr, cm⁻¹: 600, 760, 792, 875, 907, 1047, 1115, 1144, 1260, 1276, 1350, 1385, 1406, 1470, 1506, 1526, 1644 ν(C–C), ν(C–N), and σ(C–H); 2852, 2936, 2970, 3128, 3293, and 3445 ν(C–H) and ν(N–H). UV–vis (H₂O), λ_{max}, nm (ε, M⁻¹ cm⁻¹): 212 (9134), 247 (12 600), 289 (4930), 373 (1447). ¹H NMR (400 MHz, *d*₆-DMSO): δ –6.4, –17.7 ppm. X-ray diffraction quality crystals of **5a** were obtained by recrystallization in methanol.

[OsCl₂(Hind)₄]Cl (6a). Indazole (160 mg, 1.35 mmol) was added to a suspension of **2** (210 mg, 0.32 mmol) in 5 mL of hexanol-1, and the mixture was heated for 24 h at 170 °C, leading to formation of a red-brown suspension. Then, the alcohol was evaporated in vacuo at 60 °C. Addition of diethyl ether (15–20 mL) to the residue and treatment of the mixture in an ultrasound bath for 1.5 h resulted in a dirty-brown powder. The product **6a** as a yellow-greenish powder was purified by column chromatography on silica, using as eluent a mixture of CHCl₃/CH₃OH 5:1 and collecting the second fraction (*R_f* = 0.58). Yield: 12 mg, <5%. ESI-MS in MeOH (positive), *m/z*: 497.9 [OsCl₂(Hind)₂]⁺, 734 [OsCl₂(Hind)₄]⁺; ESI-MS in MeOH (negative), *m/z*: 495.9 [OsCl₂(Hind)₂–2H]⁻, 731.9 [OsCl₂(Hind)₄–2H]⁻. ¹H NMR (400 MHz, *d*₆-DMSO): δ 7.39, 6.28, 5.83, 4.69, 2.77, –24 ppm. Red crystals of **6a**·CH₃OH·H₂O suitable for X-ray structure analysis were obtained from a CH₃OH/hexane system.

trans-[OsCl₂(Him)₄]Cl (7a) and cis-[OsCl₂(Him)₄]Cl (8). Imidazole (60.5 mg, 0.89 mmol) was added to a suspension of **3** (108.1 mg, 0.19 mmol) in isoamyl alcohol (4 mL). The mixture was heated at 130 °C for 47 h. Then, the isoamyl alcohol was evaporated under reduced pressure at 60 °C, the residue was washed with diethyl ether, and dried in vacuo. The solid was dissolved in a CHCl₃/CH₃OH mixture (2:1) and passed through a silica column, using CHCl₃/CH₃OH 2:1 as eluent. The second (*R_f* = 0.7) and the third (*R_f* = 0.5) fraction were collected. Removing the volatile components of the second fraction under reduced pressure followed by vacuum sublimation of imidazole as contaminant at 90 °C afforded the red solid of **7a**. Yield: 68.2 mg, 60%. Dark-red **8** was isolated from the third fraction after removing the solvent under reduced pressure. Yield: 3–5 mg, <4%. X-ray diffraction quality crystals of **7a** and **8** were obtained from methanol solutions of complexes saturated with diethyl ether.

Complex 7a. Anal. Calcd for C₁₂H₁₆Cl₃N₈Os (*M_r* = 568.9 g/mol): C, 25.33; H, 2.83; N, 19.69. Found: C, 25.27; H, 2.59; N, 19.41. ESI-MS in MeOH (positive), *m/z*: 398.2 [OsCl₂(Him)₂]⁺, 534.3 [OsCl₂(Him)₄]⁺, ESI-MS in MeOH (negative), *m/z*: 465.4 [OsCl₂(Him)₃–2H]⁻, 532.0 [OsCl₂(Him)₄–2H]⁻. IR spectrum in KBr, cm⁻¹: 614, 658, 729, 743, 769, 840, 1074, 1100, 1144, 1182, 1264, 1330, 1444, 1492, 1508, 1548, 1560, 1578, and 1686 ν(C–C),

Table 1. Crystal Data and Details of Data Collection for **5a**, **6a**, **7a**, **8**, and **9a**

complex	5a	6a ·CH ₃ OH·H ₂ O	7a	8	9a ·CH ₃ OH·(C ₂ H ₅) ₂ O
empirical formula	C ₁₂ H ₁₆ Cl ₃ N ₈ Os	C ₂₉ H ₃₀ Cl ₃ N ₈ O ₂ Os	C ₁₂ H ₁₆ Cl ₃ N ₈ Os	C ₁₂ H ₁₆ Cl ₃ N ₈ Os	C ₃₃ H ₃₈ Cl ₃ N ₈ O ₂ Os
fw	568.88	819.16	568.88	568.88	875.26
space group	<i>P</i> $\bar{1}$	<i>C2/c</i>	<i>C2/c</i>	<i>Cm</i>	<i>P2₁/n</i>
<i>a</i> , Å	7.9101(2)	16.9910(4)	9.6110(3)	11.229(2)	15.7469(4)
<i>b</i> , Å	8.4109(2)	11.1273(4)	18.9329(9)	12.259(3)	13.6976(4)
<i>c</i> , Å	14.6494(4)	16.6057(4)	9.6818(3)	7.0080(14)	16.5585(5)
α , deg	102.690(2)				
β , deg	99.886(1)	97.557(2)	90.016(2)	104.11(3)	93.710(2)
γ , deg	110.743(2)				
<i>V</i> , Å ³	884.54(4)	3112.27(15)	1761.74(11)	935.6(3)	3564.10(17)
<i>Z</i>	2	4	4	2	4
λ , Å	0.71073	0.71073	0.71073	0.71073	0.71073
ρ_{calcd} , g cm ⁻³	2.136	1.748	2.145	2.019	1.631
cryst size, mm ³	0.25 × 0.15 × 0.12	0.20 × 0.12 × 0.10	0.30 × 0.12 × 0.12	0.12 × 0.06 × 0.01	0.30 × 0.20 × 0.20
<i>T</i> , K	100	100	100	100	100
R1 ^a	0.0129	0.0222	0.0115	0.0155	0.0262
wR2 ^b	0.0296	0.0546	0.0306	0.0354	0.0593
GOF ^c	1.026	1.081	1.088	1.016	1.001

^a R1 = $\sum ||F_o| - |F_c|| / \sum |F_o|$. ^b wR2 = $\{ \sum [w(F_o^2 - F_c^2)^2] / \sum [w(F_o^2)^2] \}^{1/2}$. ^c GOF = $\{ \sum [w(F_o^2 - F_c^2)^2] / (n - p) \}^{1/2}$, where *n* is the number of reflections and *p* is the total number of parameters refined.

$\nu(\text{C}-\text{N})$ and $\sigma(\text{C}-\text{H})$; 2586, 2622, 2871, 2975, 3083, and 3170 $\nu(\text{C}-\text{H})$ and $\nu(\text{N}-\text{H})$. UV-vis (H₂O), λ_{max} , nm (ϵ , M⁻¹ cm⁻¹): 207 (59 705), 216 (58 039), 252 sh (19 354), 296 (11 495), 384 (821). ¹H NMR (400 MHz, *d*₆-DMSO): δ 9.85, 5.78, -8.59, -14.92 ppm.

Complex 8. ESI-MS in MeOH (positive), *m/z*: 398.2 [OsCl₂(Him)₂]⁺, 534.3 [OsCl₂(Him)₄]⁺, ESI-MS in MeOH (negative), *m/z*: 396.3 [OsCl₂(Him)₂-2H]⁻, 465.8 [OsCl₂(Him)₃-2H]⁻, 530.0 [OsCl₂(Him)₄-2H]⁻. ¹H NMR (400 MHz, *d*₆-DMSO): δ 15.88, 11.45, 8.97, 4.14, -4.16, -13.0, -15.7, -17.97 ppm.

trans-[OsCl₂(Hbzim)₄]Cl (9a). Benzimidazole (163 mg, 1.38 mmol) was added to a suspension of **4** (214.6 mg, 0.34 mmol) in hexanol-1 (5 mL), and the mixture was heated at 160 °C for 24 h to give a yellow-brown solution. Then, the alcohol was evaporated under reduced pressure at 60 °C. Addition of diethyl ether (15–20 mL) to the residue, and treatment of the mixture in an ultrasound bath for 1.5 h resulted in a dirty-yellow solid. This was filtered off, dried in vacuo and purified by column chromatography on silica using as eluent a mixture of CHCl₃/CH₃OH 4:1 and collecting the third fraction (*R*_f = 0.48) or CHCl₃/CH₃OH 3:1 (*R*_f = 0.67). The product of the composition **9a**·CH₃OH·(C₂H₅)₂O, crystallized as dark-orange crystals by diffusion of diethyl ether into the methanol solution of **9a**, was filtered off, washed with diethyl ether, and dried under nitrogen atmosphere at 140 °C for 1 h. Yield: 180 mg, 70%. A yellow powder of **9a**·*n*(C₂H₅)₂O was obtained after evaporating volatile components of the third fraction, addition of diethyl ether to the remaining residue, and treatment of this mixture in an ultrasound bath. Anal. Calcd for C₂₈H₂₄Cl₃N₈Os (*M*_r = 769.13 g/mol): C, 43.72; H, 3.15; N, 14.57. Found: C, 43.56; H, 3.08; N, 14.47. ESI-MS in MeOH (positive), *m/z*: 498.2 [OsCl₂(Hbzim)₂]⁺, 734.3 [OsCl₂(Hbzim)₄]⁺; ESI-MS in MeOH (negative), *m/z*: 496.3 [OsCl₂(Hbzim)₂-2H]⁻, 732.1 [OsCl₂(Hbzim)₄-2H]⁻. IR spectrum in KBr, cm⁻¹: 428, 456, 549, 615, 697, 739, 760, 775, 846, 857, 884, 975, 1012, 1113, 1144, 1185, 1250, 1264, 1306, 1350, 1421, 1464, 1493, 1508, 1594, 1619, 1708, and 1774 $\nu(\text{C}-\text{C})$, $\nu(\text{C}-\text{N})$ and $\sigma(\text{C}-\text{H})$; 2837, 2911, 2982, 3102, 3133, and 3375 $\nu(\text{C}-\text{H})$ and $\nu(\text{N}-\text{H})$. UV-vis (H₂O), λ_{max} , nm (ϵ , M⁻¹ cm⁻¹): 215 (116 635), 240 sh (55 784), 294 (31 907), 300 (31 884), 312 sh (15 683), 379 (4089). ¹H NMR (400 MHz, *d*₆-DMSO): δ 9.2, 8.0, 5.12, 3.96 ppm.

Physical Measurements. Elemental analyses were carried out at the Microanalytical Service of the Institute of Physical Chemistry of the University of Vienna. UV-vis spectra were recorded on a

PerkinElmer Lambda 20 UV-vis spectrophotometer, using samples dissolved in methanol (**1–4**) and water (**5a**, **7a**, and **9a**) at 298 and 310 K. The aqueous solution behavior of **5a**, **7a**, and **9a** with respect to hydrolysis was studied at 298 and 310 K over 24–72 h by UV-vis spectroscopy (**5a**, **7a**, and **9a**) and ¹H NMR spectroscopy (**5a**). The interaction of **5a** with 9-methyladenine (1:1.5) was studied by ¹H NMR spectroscopy in aqueous phosphate buffer (pH 6.0, 310 K) over 72 h. Infrared spectra were obtained from KBr pellets with a PerkinElmer FTIR 2000 instrument (4000–400 cm⁻¹). Electrospray ionization mass spectrometry was carried out with a Bruker Esquire 3000 instrument (Bruker Daltonic, Bremen, Germany) in methanol (**5a–7a**, **8**, and **9a**) and water (**5a**). Expected and experimental isotope distributions were compared. The ¹H NMR spectra were recorded at 400.13 MHz on a Bruker DPX400 (Ultraschield™ Magnet) spectrometer. Cyclic voltammograms were measured in a two-compartment three-electrode cell using a 1.0 mm diameter glassy-carbon disk working electrode, probed by a Luggin capillary, and connected to a silver-wire pseudoreference electrode, and a platinum auxiliary electrode. Measurements were performed at room temperature, using an EG & G PARC 273A potentiostat/galvanostat. Deaeration of solutions was accomplished by passing a stream of argon through the solution for 10 min prior to the measurements and then maintaining a blanket atmosphere of argon over the solution during the measurements. The potentials were measured in 0.2 M phosphate buffer solutions (pH 7.0) (**7a**, **9a**) and in acetonitrile (0.15 M [*n*Bu₄N][BF₄]/CH₃CN) (**5a**, **6a**, **9a**), using as internal standards methyl viologen (*E*_{1/2}^{ox} = -0.44 V vs NHE in water)²⁹ and ferrocene (*E*_{1/2}^{ox} = 0.69 V vs NHE in acetonitrile)³⁰ respectively, and are quoted relative to NHE.

Crystallographic Structure Determination. X-ray diffraction measurements were performed on a Bruker X8 APEXII CCD diffractometer. Single crystals were positioned at 40 mm from the detector, and 2798, 1490, 1920, 1282, and 1724 frames were measured, each for 15, 60, 7, 80, and 2 s over 1° scan width for

(29) Guedes da Silva, M. F. C.; Pombeiro, A. J. L.; Geremia, S.; Zangrando, E.; Calligaris, M.; Zinchenko, A. V.; Kukushkin, V.; Yu, J. *Chem. Soc., Dalton Trans.* **2000**, 1363–1371.

(30) Barrette, W. C., Jr.; Johnson, H. W., Jr.; Sawyer, D. T. *Anal. Chem.* **1984**, *56*, 1890–1898.

5a, **6a**, **7a**, **8**, and **9a**, correspondingly. The data were processed using *SAINT* software.³¹ Crystal data, data collection parameters, and structure refinement details are given in Table 1.

The structures were solved by direct methods and refined by full-matrix least-squares techniques. Non-hydrogen atoms were refined with anisotropic displacement parameters. Hydrogen atoms were placed at calculated positions and refined as riding atoms in the subsequent least-squares model refinements. The isotropic thermal parameters were estimated to be 1.2 times the values of the equivalent isotropic thermal parameters of the non-hydrogen atoms to which hydrogen atoms are bonded. One of the imidazole ligands in **8** was found to be disordered over 2 mirror-related positions. Attempts to solve the structure in the space group *C2/c* ended up with more severe disorder and a higher R1 value. The following computer programs were used: structure solution, *SHELXS-97*;^{32a} refinement, *SHELXL-97*;^{32b} molecular diagrams, *ORTEP*; computer: Pentium IV. Scattering factors were taken from the literature.³³

Cell Lines and Culture Conditions. Human A549 cells (non-small cell lung carcinoma) and SW480 cells (adenocarcinoma of the colon) were kindly provided by Brigitte Marian, Institute of Cancer Research, Medical University of Vienna, Austria. CH1 cells originate from an ascites sample of a patient with a papillary cystadenocarcinoma of the ovary and were kindly donated by Lloyd R. Kelland, CRC Center for Cancer Therapeutics, Institute of Cancer Research, Sutton, UK. Cells were grown in 75 cm² culture flasks (Iwaki/Asahi Technoglass) as adherent monolayer cultures in complete culture medium, i.e., Minimal Essential Medium (MEM) supplemented with 10% heat-inactivated fetal bovine serum, 1 mM sodium pyruvate, 4 mM L-glutamine and 1% non-essential amino acids (100 ×) (all purchased from Sigma-Aldrich). Cultures were maintained at 37 °C in a humidified atmosphere containing 5% CO₂.

Cytotoxicity Tests in Cancer Cell Lines. Cytotoxicity was determined by means of the colorimetric MTT assay (MTT = 3-(4,5-dimethyl-2-thiazolyl)-2,5-diphenyl-2H-tetrazolium bromide, purchased from Fluka). For this purpose, cells were harvested from culture flasks by trypsinization and seeded in 100 μL aliquots in complete culture medium into 96-well microculture plates (Iwaki/Asahi Technoglass). Cell densities of 4.0 × 10³ cells/well (A549), 1.5 × 10³ cells/well (CH1), and 2.5 × 10³ cells/well (SW480) were chosen in order to ensure exponential growth throughout drug exposure. Cells were allowed to settle for 24 h, followed by the addition of dilutions of the test compounds in 100 μL/well complete culture medium and incubation for 96 h. At the end of exposure, drug solutions were replaced by 100 μL/well RPMI 1640 culture medium (supplemented with 10% heat-inactivated fetal bovine serum) plus 20 μL/well MTT solution in phosphate-buffered saline (5 mg/ml PBS). After incubation for 4 h, medium was removed, and the reduced formazan product formed by the metabolic activity of vital cells was dissolved in 150 μL DMSO per well. Optical densities at a wavelength of 550 nm were measured with a microplate reader (Tecan Spectra Classic), using a reference wavelength of 690 nm to correct for unspecific absorption. The quantity of vital cells was expressed in terms of *T/C* values by

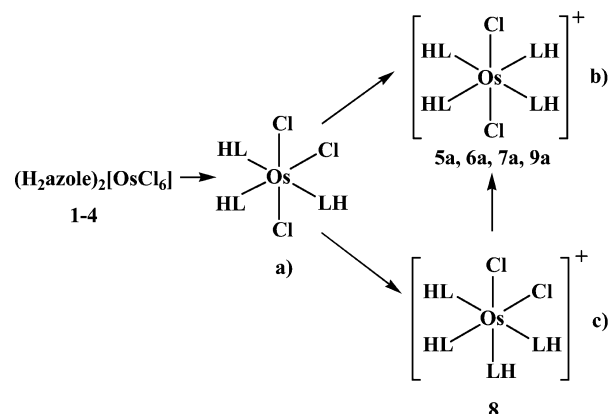
(31) *SAINT-Plus (Version 7.06a) and APEX2*; Bruker-Nonius AXS Inc.: Madison, Wisconsin, USA, 2004.

(32) (a) Sheldrick, G. M. *SHELXS-97, Program for Crystal Structure Solution*; University of Göttingen: Göttingen, Germany, 1997. (b) Sheldrick, G. M. *SHELXS-97, Program for Crystal Structure Refinement*; University of Göttingen: Göttingen, Germany, 1997.

(33) *International Tables for X-ray Crystallography*; Kluwer Academic Press: Dordrecht, The Netherlands, 1992; Vol. C, Tables 4.2.6.8 and 6.1.1.4.

(34) Chiorescu, I.; Stepanenko, I. N. Manuscript in preparation.

Scheme 1. Transformation pathways of **1–4** into **5a**, **6a**, **7a**, **8**, and **9a**: a) *mer*-[OsCl₃(Hazole)₃], b) *trans*-[OsCl₂(Hazole)₄]Cl (**5a**, **6a**, **7a**, **9a**), c) *cis*-[OsCl₂(Hazole)₄]Cl (**8**)



comparison to untreated control microcultures, and IC₅₀ values were calculated from concentration-effect curves by interpolation. Evaluation is based on means from at least three independent experiments, each comprising six replicates per concentration level.

Results and Discussion

Synthesis. $(\text{H}_2\text{azole})_2[\text{Os}^{\text{IV}}\text{Cl}_6]$ (**1–4**) were obtained by reaction of $[(\text{DMSO})_2\text{H}]_2[\text{Os}^{\text{IV}}\text{Cl}_6]$ with azole heterocycles in 1:3 molar ratio in dry ethanol at room temperature in 79–97% yields. Replacement of chlorido ligands in $[\text{OsCl}_6]^{2-}$ by azole heterocycles was realized under prolonged heating of $(\text{H}_2\text{azole})_2[\text{OsCl}_6]$ with the corresponding azole in 1:4 molar ratio in isoamyl alcohol (130 °C for **7a**, **8**) or hexanol-1 (160–170 °C for **5a**, **6a**, **9a**) to generate *trans*- $[\text{OsCl}_2(\text{Hazole})_4]\text{Cl}$ in 50–70% yields (**5a**, **7a**, **9a**) and <5% yield (**6a**). The synthesis of **6a** is accompanied by concurrent reactions, which resulted in many fractions difficult to separate by column chromatography and finally in minor yield of the desired product.

The synthesis of this family of compounds proceeds in several steps including reduction of Os^{IV} to Os^{III} and inevitable formation of *mer*- $[\text{OsCl}_3(\text{Hazole})_3]$ (Scheme 1), which can be detected in the reaction mixture along with the main product by TLC. The yield of *mer*- $[\text{Os}^{\text{III}}\text{Cl}_3(\text{Hazole})_3]$ can be significantly increased when the amount of azole heterocycle used relative to the amount of $(\text{H}_2\text{azole})_2[\text{Os}^{\text{IV}}\text{Cl}_6]$ is reduced and the reaction is carried out under milder conditions. The reaction pathways to meridional isomers were proposed and will be discussed in another work.³⁴ We note here the key role of the *mer*-isomer of $[\text{Os}^{\text{III}}\text{Cl}_3(\text{Hazole})_3]$ in the formation of $[\text{Os}^{\text{III}}\text{Cl}_2(\text{Hazole})_4]\text{Cl}$ compounds.

The fourth azole heterocycle coordinates to osmium upon substitution of the chlorido ligand, which is in the trans position to the azole ligand in *mer*- $[\text{OsCl}_3(\text{Hazole})_3]$. The substitution of one of the two mutually trans-arranged chlorido ligands is less favored (<4% yield for **8**) and was observed only for imidazole as a less bulky and strongest net electron-donor ligand (Scheme 1).

It should be noted that the synthesis of ruthenium species **5b**, **7b**, and **9b** was performed under mild conditions, starting from $[\text{RuCl}_3(\text{EtSph})_3]$ (for imidazole derivative) or $(\text{H}_2\text{azole})-$

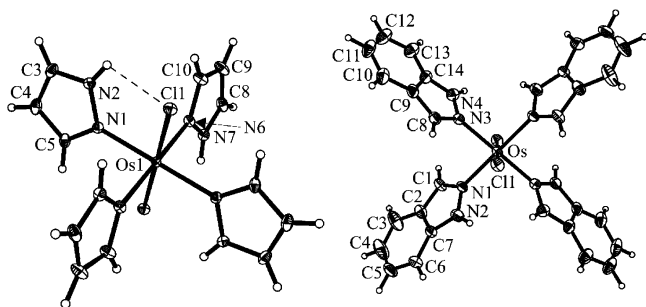


Figure 1. ORTEP plots of the first crystallographically independent cation in *trans*-[OsCl₂(Hpz)₄]Cl (**5a**) [left] and of the complex cation in *trans*-[OsCl₂(Hind)₄]Cl (**6a**) [right] with the atom-numbering schemes. Thermal displacement ellipsoids are drawn at the 50% probability level. Selected bond lengths (Å) and angles (deg) for **5a** and **6a**, correspondingly: Os1–C11 2.3722(4), Os1–C12 2.3591(4), Os1–N1 2.0657(14), Os1–N6 2.0649(13), N6–Os–N1 89.05(5), N6–Os–C11 90.94(4), N1–Os–C11 89.30(4), $\Theta_{\text{C11–Os1–N1–N2}}$ 25.42(12), $\Theta_{\text{C11–Os1–N6–N7}}$ 161.11(12); Os–C11 2.3477(9), Os–N1 2.073(3), Os–N3 2.075(3), N1–Os–N3 86.48(11), N1–Os–C11 89.86(9), N3–Os–C11 90.04(9), $\Theta_{\text{C11–Os1–N1–N2}}$ –30.7(3), $\Theta_{\text{C11–Os1–N3–N4}}$ 155.7(3).

[RuCl₄(Hazole)₂] (where Hazole = Hpz, Hbzim).¹⁹ Likewise, the *mer*-[RuCl₃(Hazole)₃] was an intermediate in the synthesis of *trans*-[RuCl₂(Hazole)₄]Cl. Starting from (H₂ind)-[RuCl₄(Hind)₂] and indazole in refluxing aqueous ethanol, *trans*-[RuCl₂(Hind)₄] was obtained. Oxidation of the latter with hydrogen peroxide in methanol in the presence of hydrochloric acid and indazole resulted in **6b**.¹⁷ Formation of *cis*-[RuCl₂(Hazole)₄]Cl or isomerization of *trans*-[RuCl₂(Hazole)₄] into the *cis* isomer has not been observed yet.

The ruthenium compounds are kinetically more labile toward ligand exchange or isomerization than the analogous osmium species. The minor yield of *cis*-[OsCl₂(Him)₄]Cl (**8**) produced under harsh conditions along with predominant formation of the *trans* isomer **7a** suggests that the transient *cis* isomers in the case of ruthenium were not discovered because of their quick isomerization into *trans* species.

Crystal Structures. The structures of the complexes reported herein are of interest because of the paucity of documented X-ray diffraction data on osmium(III) complexes and especially on osmium(III)-azole derivatives. Reported data on the latter are confined to TpOs^{III}(Him)Cl₂³⁵ and [Os^{III}Cl₃(Hazole)₃], where Hazole = pyrazole, indazole, imidazole, or benzimidazole.^{34,36} In addition, these are to our knowledge the first structures of osmium compounds containing four azole and two chlorido ligands at the metal center.³⁷ The crystal structures of **5a–7a** and **9a** consist of [OsCl₂(Hpz)₄]⁺, [OsCl₂(Hind)₄]⁺, [OsCl₂(Him)₄]⁺, and [OsCl₂(Hbzim)₄]⁺ cations, respectively, and Cl[–] anions. Cocrystallized solvent molecules were found in the crystal structures of **6a** (disordered CH₃OH and H₂O) and **9a** (CH₃OH and (C₂H₅)₂O). Figure 1 displays perspective views of the [OsCl₂(Hpz)₄]⁺ and [OsCl₂(Hind)₄]⁺ cations and Figure 2 those of [OsCl₂(Him)₄]⁺ and [OsCl₂(Hbzim)₄]⁺

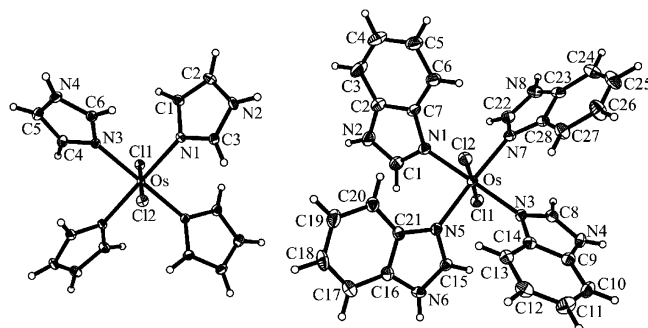


Figure 2. ORTEP plots of the complex cations in *trans*-[OsCl₂(Him)₄]Cl (**7a**) [left] and *trans*-[OsCl₂(Hbzim)₄]Cl (**9a**) [right] with the atom-numbering schemes. Thermal displacement ellipsoids are drawn at the 50% probability level. Selected bond lengths (Å) and angles (deg) in **7a** and **9a**, respectively: Os–C11 2.3558(5), Os–C12 2.3576(5), Os–N1 2.0712(14), Os–N3 2.0693(14), N1–Os–N3 89.87(6), N1–Os–N1' 179.14(7), N1–Os–C11 90.43(3), N1–Os–C12 89.57(3), $\Theta_{\text{C11–Os–N1–C1}}$ 45.68(13), $\Theta_{\text{C11–Os–N3–C4}}$ 50.13(13); Os–C11 2.3683(8), Os–C12 2.3479(8), Os–N1 2.081(3), Os–N3 2.071(3), Os–N5 2.076(3), Os–N7 2.089(3), N1–Os–N7 92.04(11), N1–Os–N3 177.97(11), N1–Os–C11 88.72(8), N1–Os–C12 90.26(8), $\Theta_{\text{C11–Os–N1–C1}}$ 51.2(3), $\Theta_{\text{C11–Os–N5–C15}}$ 49.5(3), $\Theta_{\text{C11–Os–N3–C8}}$ 44.3(3), $\Theta_{\text{C11–Os–N7–C22}}$ 40.9(3).

cations. Selected bond lengths (Å) and angles (deg) are quoted in the legends to Figures 1 and 2. **7a** crystallized in the monoclinic space group *C2/c* and is isostructural (Figure S1 in the Supporting Information) with the related ruthenium compound **7b**.¹⁹

The osmium(III) ions in [OsCl₂(Hpz)₄]⁺, [OsCl₂(Hind)₄]⁺, [OsCl₂(Him)₄]⁺, and [OsCl₂(Hbzim)₄]⁺ of **5a–7a** and **9a** have the expected distorted octahedral coordination geometry, with four azole heterocycles bound through their nitrogen atoms in the equatorial plane and two chloride ligands in axial positions. A propeller-like arrangement of the tetrazole core, formed on the tilt of the azole rings with respect to the OsN₄ plane to reduce the mutual repulsions, is characteristic for the cations in **5a–7a** and **9a**. The pitch of the four azole planes varies between 18.8 and 20.9° in the first crystallographically independent complex cation of **5a**, and between 24.6 and 34.8° in the second, 24.4 and 31.2° in **6a**, 42.0 and 44.9° in **7a**, and between 43.8 and 48.8° in **9a**. The *trans*-coordinated pyrazole and indazole ligands in **5a** and **6a**, correspondingly, are parallel to one another, whereas imidazole and benzimidazole planes are almost perpendicular to one another in **7a** and **9a**, respectively.

The average Os–Cl bond lengths [2.365(7) (**5a**), 2.3477(9) (**6a**), 2.3567(9) (**7a**), and 2.358(10) Å (**9a**)] are well comparable to those found in (H₂im)[*trans*-OsCl₄(Him)-(DMSO)] [2.3627(11) Å]²⁶ and in *mer*-[OsCl₃(NH₃)₂(Me₂S)] [2.368(8) Å].²⁹ The average Os–N bond in **5a–7a** and **9a** [2.0653(4), 2.074(3), 2.0703(9), and 2.079(5) Å, correspondingly] is well comparable with the average Ru–N bond in the related ruthenium complexes *trans*-[RuCl₂(Hpz)₄]Cl (**5b**), *trans*-[RuCl₂(Hind)₄]Cl (**6b**), *trans*-[RuCl₂(Him)₄]Cl (**7b**), and *trans*-[RuCl₂(Hbzim)₄]Cl (**9b**) [2.0603(24), 2.0705(3), 2.0685(3), and 2.0771(36) Å, correspondingly]^{17,19} and is significantly shorter than similar bonds *trans* to sulfur-bound DMSO in the osmium(II) complexes *trans,cis,cis*-[OsCl₂(Hind)₂(DMSO)₂] and *trans,cis,cis*-[OsCl₂(Hpz)₂(DMSO)₂] at 2.130(4), 2.137(4), and 2.1202(17), 2.1365(17)

(35) Bennett, B. K.; Pitteri, S. J.; Pilobello, L.; Lovell, S.; Kaminsky, W.; Mayer, J. M. *J. Chem. Soc., Dalton Trans.* **2001**, 3489–3497.

(36) Chiorescu, I.; Stepanenko, I. N.; Arion, V. B.; Krokhnin, A. A.; Keppler, B. K. *J. Biol. Inorg. Chem.* **2007**, *12* (Suppl 1), S226.

(37) CSD version 5.29; November 2007.

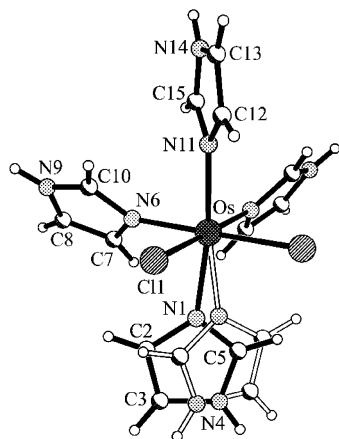


Figure 3. The structure of the cation in *cis*-[OsCl₂(Him)₄]Cl (**8**), showing the atom-numbering scheme. Selected bond lengths (Å) and angles (deg): Os–Cl1 2.371(2), Os–N1 2.092(10), Os–N6 2.050(6), Os–N11 2.069(9), N6–Os–N11 88.1(2), N11–Os–N1 172.2(3), N6–Os–Cl1 88.65(13), N1–Os–Cl1 84.7(3), N1ⁱ–Os–Cl1 95.5(3), ∠_{Cl1–Os–N1–C2} 54.7(8), ∠_{Cl1–Os–N6–C7} 126.8(5), and ∠_{Cl1–Os–N11–C12} 45.58(6); symmetry code: *i* = *x*, *−y*, *z*.

Å, correspondingly.³⁸ Like for ruthenium congeners, in *trans*-[OsCl₂(Hazole)₄]Cl the average M–N bond lengths are in the following rank order (**5a** < **6a**) and (**7a** < **9a**), which agrees well with the relative electron-donor character of the corresponding N-ligand pairs [*E_L*(Hind) > *E_L*(Hpz) and *E_L*(Hbzim) > *E_L*(Him)] and their basicities [*pK_a*(H₂ind⁺) < *pK_a*(H₂pz⁺) and *pK_a*(H₂bzim⁺) < *pK_a*(H₂im⁺)]^{18,19,39–41}

Of note are also the intramolecular hydrogen bonding interactions N2–H···Cl1 (Figure 1) and N17–H···Cl2 in two crystallographically independent cations of **5a** [N2–H 0.880, H···Cl1 2.681, N2···Cl1 3.159 Å, ∠N2HC11 115.34°; N17–H 0.880, H···Cl2 2.741, N17···Cl2 3.176 Å, ∠N17HC12 111.88°]. In addition, the crystal structures of **5a**, **6a**, and **9a** are stabilized by interionic hydrogen bonds of the type N–H···Cl (Tables S1–S3 in the Supporting Information). Each chloride ion in **7a** forms four hydrogen bonds with four imidazole rings of four neighboring complex cations (Figure S2 in the Supporting Information).

8 crystallized in the monoclinic space group *Cm*. The crystal structure of **8** consists of [OsCl₂(Him)₄]⁺ cations and Cl[−] anions. Figure 3 displays a perspective view of the [OsCl₂(Him)₄]⁺ cation. Selected bond lengths (Å) and angles (deg) are quoted in the legend to Figure 3.

The osmium(III) ion in *cis*-[OsCl₂(Him)₄]⁺ has the expected distorted octahedral coordination geometry, with two *cis*-arranged chlorido ligands and two imidazole ligands in equatorial positions and other two imidazoles in axial positions, one of which was found disordered over two positions with 50:50% occupancy. The Os–Cl bond length

of 2.371(2) Å is significantly longer than the Os–Cl bond in *trans*-[OsCl₂(Him)₄]⁺ [2.3567(9) Å], (H₂im)[*trans*-OsCl₄(Him)(DMSO)] [2.3627(11) Å],²⁶ or in *mer*-[OsCl₃(NH₃)₂(Me₂S)] [2.368(8) Å].²⁹ The average Os–N bond in **8** [2.071(21) Å] is well comparable with the average Ru–N bond in the related ruthenium complexes *trans*-[RuCl₂(Him)₄]Cl (**7b**) and *trans*-[RuCl₂(Hbzim)₄]Cl (**9b**) [2.0685(3) Å and 2.0771(36) Å, correspondingly],¹⁹ but slightly longer than the average Ru–N bond in *trans*-[RuCl₂(Hind)₄] [2.0639(1) Å].¹⁷

UV–vis Spectra. The electronic absorption spectra of the aqueous solutions of **5a**, **7a**, and **9a** are characterized by four absorption bands with maxima within 200–215, 240–252, 288–300, and 373–380 nm. The first three absorptions (the second band of **7a** and **9a** is a shoulder) are overlapping bands due to intraligand transitions of coordinated azole heterocycles and charge-transfer (CT) bands. The UV–vis spectrum of **9a** has the third benzenoid band.⁴² The fourth band is also attributed to CT transitions. Their extinction coefficients are in the range from 820 to 4089 M^{−1} cm^{−1}, which are too intense for pure d–d transitions. The d–d bands of osmium(III) are often overlapped with the low-energy CT absorptions since the low-spin osmium(III) has large spin–orbital contribution from intraconfigurational transitions. Because of the decrease of CT transition energy in the series **5a**–**9a**–**7a** bathochromic shifts from 289 to 296 and from 373 to 384 nm for the third and fourth bands were observed.

The analogous ruthenium compounds have the same character of UV–vis spectra,¹⁹ but because of the stronger ligand field splitting for a third-row transition metal CT bands of [OsCl₂(Hazole)₄]Cl are blue-shifted. CT bands of [RuCl₂(Hazole)₄]Cl were described as LMCT transitions and, in contrast to the investigated complexes (**5a**, **7a**, and **9a**), they are blue-shifted with increasing basicity and electron donor properties of the N-ligands ([RuCl₂(Hpz)₄]Cl, 401 nm; [RuCl₂(Hbzim)₄]Cl, 363 nm; [RuCl₂(Him)₄]Cl, 346 nm).¹⁹ For comparison, the compounds (H₂azole)[*trans*-OsCl₄-(Hazole)(DMSO)] did not show a dependence of CT energy on the electron-donor character of the N-ligands.²⁶

The LMCT bands for [MCl₂(Hazole)₄]Cl are probably due to π Cl → d transitions. Besides, the electron transition from π orbitals of azole to metal d orbitals can also take place. The hole in t_{2g}⁵ configuration of the metal is presumably responsible for these low-energy transitions. MLCT d → π* (azole) transitions might also be expected.

The absence of clear correlations between the CT energy and the observed M–Cl and M–N length variation in [MCl₂(Hazole)₄]Cl can presumably be explained by the domination of some CT bands, which makes the interpretation of electronic absorption spectra difficult.

Electrochemical Study. The cyclic voltammograms of **7a**, **9a** in 0.2 M phosphate buffer (pH 7) and **5a**, **6a**, **9a** in acetonitrile (0.15 M [*n*Bu₄N][BF₄]/CH₃CN) at a carbon disk working electrode, recorded with a scan rate of 0.2 V/s,

(38) Stepanenko, I. N.; Cebrian-Losantos, B.; Arion, V. B.; Krokhin, A. A.; Nazarov, A. A.; Keppler, B. K. *Eur. J. Inorg. Chem.* **2007**, *3*, 400–411.

(39) Reedijk, J. In *Comprehensive Coordination Chemistry*; Wilkinson, G.; Gillard, R. D.; McCleverty, J. A., Eds.; Pergamon Press: Elmsford, NY, 1987; *2*, 73–98.

(40) Reisner, E.; Arion, V. B.; Keppler, B. K.; Pombeiro, A. J. L. *Inorg. Chim. Acta* **2008**, *361*, 1569–1583.

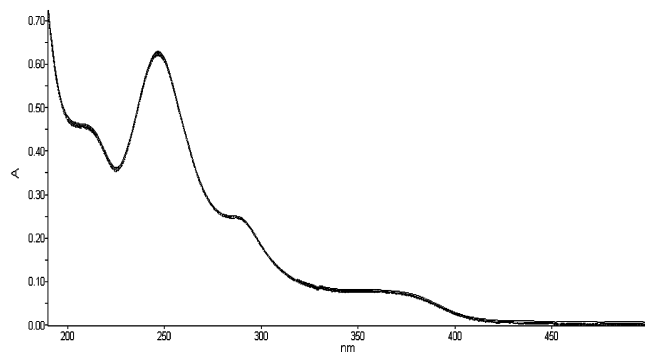
(41) Catalán, J.; Claramunt, R. M.; Elguero, J.; Laynez, J.; Menéndez, M.; Anvia, F.; Quian, J. H.; Taagepera, M.; Taft, R. W. *J. Am. Chem. Soc.* **1988**, *110*, 4105–4111.

(42) Lambert, J. B.; Shurvell, H. F.; Lightner, D. A.; Cooks, R. G. *Organic Structural Spectroscopy*; Prentice Hall: Upper Saddle River, N. J.: USA, 1998.

Table 2. Cyclic Voltammetric Data for **5a–7a** and **9a**

complex	$E_{1/2}$ (Os ^{II/III}) ^a , (ΔE_p) ^b	$E_{1/2}$ (Os ^{III/IV}) ^a , (ΔE_p) ^b	$E_{1/2}$ (Os ^{II/III}) ^c , (ΔE_p) ^b	$E_{1/2}$ (Os ^{III/IV}) ^c , (ΔE_p) ^b
5a ^d			−0.2 (70)	1.35 (60)
6a ^d			0.1 (60)	1.55 (70)
7a ^e	−1.17 (60)	0.36 (70)		
9a	−1.21 (60)	0.31 (70)	−0.4 (60)	1.1 (70)

^a Potentials $E_{1/2}$ ($E_{1/2} = (E_{pa} + E_{pc})/2$, where E_{pa} and E_{pc} are the anodic and cathodic peak potential, respectively) measured at a scan rate 0.2 V s^{-1} in 0.2 M phosphate buffer solutions (pH 7.0), using methyl viologen ($E_{1/2}^{2ox} = -0.44 \text{ V}$ vs NHE in water) as internal standard, are given in volts and quoted relative to NHE. ^b ΔE_p values ($\Delta E_p = E_{pa} - E_{pc}$) are given in millivolts. ^c Potentials are measured at a scan rate 0.2 V s^{-1} in 0.15 M $[\text{nBu}_4\text{N}][\text{BF}_4]/\text{CH}_3\text{CN}$, using ferrocene ($E_{1/2}^{ox} = 0.69 \text{ V}$ vs NHE in acetonitrile) as internal standard, and quoted relative to NHE. ^d Complex is pour soluble in phosphate buffer solution. ^e Complex is pour soluble in CH_3CN .

**Figure 4.** Multiple UV–vis spectra of aqueous solution of **5a** measured over 72 h with 1 h time interval.

display a reversible one-electron reduction wave with potential values ranging from -1.21 to -1.17 V (in phosphate buffer) or -0.4 to 0.1 V (in CH_3CN), which is assigned to the $\text{Os}^{\text{III}} \rightarrow \text{Os}^{\text{II}}$ process, and a one-electron oxidation wave with potential values ranging from 0.31 to 0.36 V (in phosphate buffer) or 1.10 to 1.55 V (in CH_3CN), which is attributed to the $\text{Os}^{\text{III}} \rightarrow \text{Os}^{\text{IV}}$ process (Table 2). The redox potentials of the complexes are in the following rank order: $E_{1/2}(\mathbf{7a}) \geq E_{1/2}(\mathbf{9a})$ (in phosphate buffer) and $E_{1/2}(\mathbf{6a}) > E_{1/2}(\mathbf{5a}) > E_{1/2}(\mathbf{9a})$ (in CH_3CN), which agrees with the relative electron-donor character of the N-ligands ($E_L(\text{Hind}) > E_L(\text{Hpz}) > E_L(\text{Hbzim}) > E_L(\text{Him})$).⁴⁰ The redox responses are characterized by a peak-to-peak separation (ΔE_p) of 60 – 70 mV and an anodic peak current (i_{pa}) that is almost equal to the cathodic peak current (i_{pc}), as expected for reversible electron-transfer processes. The one-electron nature of electron-transfer processes was verified by comparing the peak current height (i_p) with that of standard methyl viologen or ferrocene/ferrocenium couples under identical experimental conditions.

Resistance to Hydrolysis and Reactivity Toward 9-Methyladenine in Aqueous Media. The aqueous solution behavior of **5a**, **7a**, and **9a** with respect to hydrolysis was studied at 298 and 310 K over 24–72 h by UV–vis spectroscopy and in addition for **5a** by ¹H NMR spectroscopy. The complexes are quite stable in aqueous solution as can be seen from their electronic absorption spectra (Figure 4, for **5a**). Immediate hydrolysis can be excluded because of the presence of the parent peak

Table 3. Cytotoxicity of Osmium Complexes **5a**, **7a**, and **9a** and Ruthenium Complexes **5b**, **7b**, and **9b** in Three Human Cancer Cell Lines

compound	IC ₅₀ (μM) ^a		
	A549	CH1	SW480
5a	3.2 ± 0.8	1.0 ± 0.2	2.3 ± 0.2
5b	18 ± 2	2.0 ± 0.2	2.9 ± 0.2
7a	60 ± 11	39 ± 2	38 ± 2
7b	2.1 ± 0.4	7.1 ± 1.0	1.7 ± 0.3
9a	12 ± 2	2.3 ± 0.2	3.0 ± 0.6
9b	4.6 ± 0.2	9.1 ± 1.9	2.0 ± 0.1

^a 50% inhibitory concentrations in the MTT assay (96 h exposure). Values are means ± standard deviations of at least three independent experiments.

$[\text{OsCl}_2(\text{Hpz})_4]^+$ in the positive ion ESI mass spectrum of an aqueous solution of **5a**.

¹H NMR spectra of **5a** in D_2O (310 K) were monitored over 72 h. The spectra obtained immediately after dissolution of **5a** and after 72 h were identical, providing further evidence against hydrolysis of the complex in aqueous medium. ¹H NMR spectra of a mixture of **5a** and 9-methyladenine (as a DNA model base) in 1:1.5 molar ratio in phosphate buffer (pH 6.0, 310 K) were measured. The absence of a new set of signals expected for coordinated 9-methyladenine even after 72 h indicated inertness of **5a** toward the purine nucleobases under the conditions employed (Figure S3 in the Supporting Information).

Antiproliferative Activity. The osmium(III) complexes **5a**, **7a**, and **9a** as well as their ruthenium(III) analogues **5b**, **7b**, and **9b** were studied for their antiproliferative activity in three human cancer cell lines by means of the MTT assay. IC₅₀ values are listed in Table 3, and concentration–effect curves are depicted in Figure 5. All compounds have noteworthy antiproliferative effects, with IC₅₀ values in the 10^{-6} to 10^{-5} M concentration range. The cisplatin-sensitive ovarian carcinoma cell line CH1 tends to be somewhat more sensitive to these complexes than the intrinsically cisplatin-resistant cell lines A549 (non-small cell lung cancer) and SW480 (colon cancer), with the notable exception of the ruthenium complexes **7b** and **9b**. The activity pattern of these two compounds is all the more remarkable, as CH1 cells are generally chemosensitive to a broad variety of anticancer agents.

Variation of the central metal yields no uniform picture: osmium is at least slightly more favorable in the case of pyrazole complexes, whereas ruthenium results in a markedly higher antiproliferative activity in the case of imidazole complexes. Structure–activity relationships with regard to variation of the azole ligand are not uniform either. In the cisplatin-resistant cell lines (A549, SW480), activity of the osmium complexes decreases in the following rank order: **5a** (Hpz) \geq **9a** (Hbzim) $>$ **7a** (Him), whereas their ruthenium congeners rank in the reverse order. In CH1 cells, the rank order also differs between osmium and ruthenium complexes, but imidazole ligands are unfavorable in any case. All three ruthenium complexes (**5b**, **7b**, **9b**) exert lower antiproliferative effects than the indazole analogue **6b** (IC₅₀: 0.67 and 0.69 μM in CH1 and SW480 cells, respectively).¹⁷

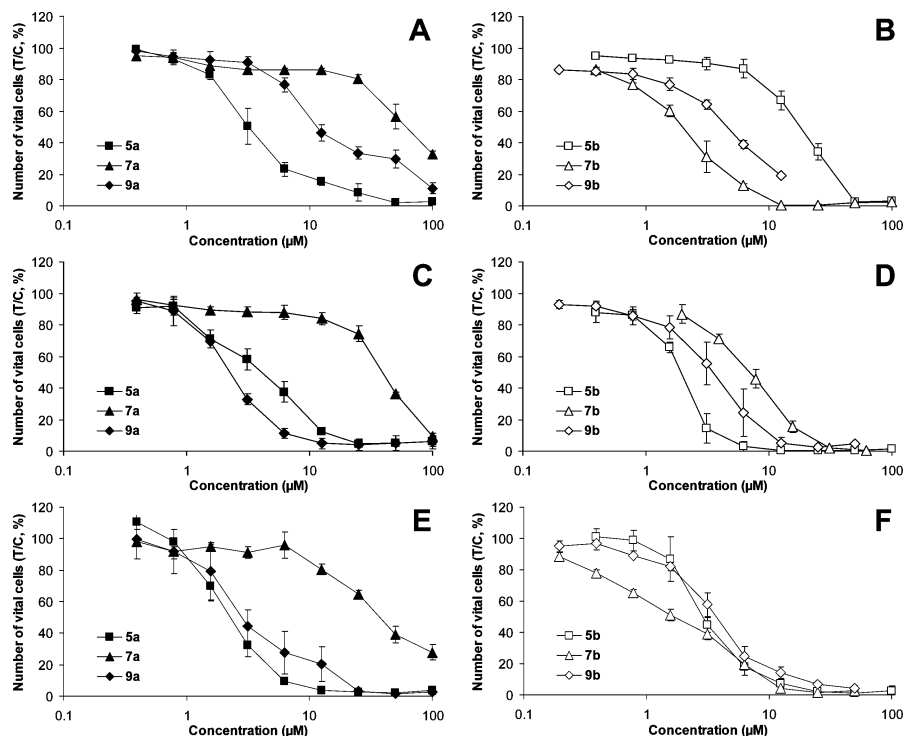


Figure 5. Concentration-effect curves of osmium complexes **5a**, **7a**, and **9a** (left panels) and ruthenium complexes **5b**, **7b**, and **9b** in A549 (A, B), CH1 (C, D) and SW480 (E, F) cells, obtained by the MTT assay (96 h exposure). Values are means \pm standard deviations of at least three independent experiments.

A fairly well correlation of reduction potentials and cytotoxic potencies observed within a homologous series of ruthenium complexes containing varying numbers of indazole and chlorido ligands¹⁷ had substantiated the concept of fine-tuning biological activity of ruthenium complexes by adjusting their ligand composition to achieve the desired redox properties and thereby stimulated the preparation of new analogues with different azole ligands in varying numbers.¹⁹ Because a number of four indazole ligands had resulted in a strong antiproliferative activity in cancer cells in vitro, we have focused here on complexes with four azole ligands. In conformity with expectations, the less easily reducible complexes with pyrazole, imidazole, and benzimidazole show lower antiproliferative activity than that reported previously for their indazole analogue. Although activities in the cisplatin-sensitive ovarian carcinoma cell line CH1 approximate a correlation with reduction potentials, any attempt to find further conclusive relationships is complicated by the fact that activities strongly depend on the cell line, however. The latter also applies to the osmium compounds, indicating that variation of the azole ligand has less predictable consequences for biological activity and that the reduction potential is not the only important parameter.

Conclusions

A $[\text{Os}^{\text{III}}\text{Cl}_2(\text{Hazole})_4]\text{Cl}$ family of complexes was prepared by reactions of $(\text{H}_2\text{azole})_2[\text{OsCl}_6]$ with the corresponding azole heterocycle. The full characterization of $[\text{OsCl}_2(\text{Hazole})_4]\text{Cl}$, both in the solid state and in solution,

permitted the elucidation of essential differences between related osmium and ruthenium complexes. Whereas their trans isomers were observed for all azole heterocycles, the formation of cis isomers was discovered only for the osmium complex with the strongest net electron-donor imidazole ligand. We found that osmium complexes, which are markedly more inert than related ruthenium compounds toward substitution reactions (hydrolysis, interaction with DNA bases), in accordance with their position in the periodic table, partially show a comparable antiproliferative activity.

$[\text{Os}^{\text{III}}\text{Cl}_2(\text{Hpz})_4]\text{Cl}$ complex showed a higher activity than the ruthenium(III) counterpart in three cell lines, whereas the osmium(III) imidazole complex is less cytotoxic than the ruthenium analogue in any case. The lack of a clear-cut correlation between antiproliferative activity and reduction potentials within the two series of $[\text{Os}^{\text{III}}\text{Cl}_2(\text{Hazole})_4]\text{Cl}$ and $[\text{Ru}^{\text{III}}\text{Cl}_2(\text{Hazole})_4]\text{Cl}$ complexes with varied azole ligands indicates that the reduction potential cannot be the main determinant factor for biological activity and that the influence of additional parameters (e.g., cellular uptake, interactions with molecular targets) is of great importance. Although synthetic limitations impeded the assay of antiproliferative activity in vitro of **5a** and cis-isomer **8**, it is worth reporting the available data, because this may inspire novel synthetic approaches to these complexes, allowing for larger scale synthesis and then evaluation of their cytotoxicity.

Acknowledgment. We thank Dr. S. Shova for helpful discussion.

Supporting Information Available: Hydrogen bonds and their geometrical parameters in **5a**, **6a**, **9a**, superposition of crystallographically independent halves of **7a** and **7b**, N–H···Cl hydrogen bonding interactions in **7a**, ¹H NMR spectra of **5a** with 9-methyladenine, assignment of UV–vis spectra of **1–4**, description of IR spectra of **1–4**, **5a**, **7a**, **9a**, and comparison of those with free azoles,

X-ray crystallographic files in CIF format for **5a–7a**, **8**, and **9a**. This material is available free of charge via the Internet at <http://pubs.acs.org>.

IC8006958